Analysis and modeling of a pneumatic artificial muscle system

Vinh-Phuc Tran[1,2,3], Nhut-Thanh Tran[1], Chi-Ngon Nguyen[1], Chanh-Nghiem Nguyen[1,2]

[1]Faculty of Automation Engineering, Can Tho University, Can Tho, Vietnam
[2]Automation Laboratory, Can Tho University, Can Tho, Vietnam
[3]Faculty of Mechanical Engineering Technology, Vinh Long University of Technology Education, Vinh Long, Vietnam

Article Info	ABSTRACT

Hysteresis is a common challenge in achieving precise position control of pneumatic artificial muscles (PAMs). Accurate modeling of this phenomenon is essential for the development of efficient PAM control systems. This study evaluates four mathematical models for modeling PAM dynamics: Nonlinear AutoRegressive with eXogenous inputs (NARX), Box-Jenkins (BJ), Prandtl-Ishlinskii (PI), and second-order underdamped system and one zero (P2UZ). To assess the effectiveness of these models, experiments were conducted with reference input signals of varying amplitudes. The accuracy and goodness of fit of these models were evaluated based on root mean square error (RMSE) and coefficient of determination. Results show that the P2UZ model achieved the highest fitness (97.15%) and the lowest RMSE (1.80 mm), followed closely by the NARX model with 96.83% fitness and an RMSE of 1.90 mm. The PI and BJ models demonstrated lower performance, with the BJ model showing the lowest fitness (90.79%) and the highest RMSE (3.25 mm). These findings provide valuable insights for improving PAM control and PAM-based automation systems by highlighting the strengths and limitations of each model.
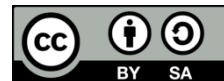
Corresponding Author:

Chanh-Nghiem Nguyen
Faculty of Automation Engineering, Can Tho University
Campus II, 3/2 Street, Ninh Kieu district, Can Tho City, Vietnam.
Email: ncnghiem@ctu.edu.vn

1. INTRODUCTION

Pneumatic artificial muscles (PAMs) have demonstrated significant potential in various engineering fields, particularly in robotics, assistive devices, and automation systems [1]–[3]. Their exceptionally high force-to-weight and torque-to-weight ratios [4] make them attractive for applications in electrical, electronics, control, telecommunications, and computer engineering [5]–[7]. The PAM consists of three main components: an outer braided fiber, an internal rubber ball, and a sealed cover with an air intake/exhaust port. When compressed air is supplied to the PAM, it shrinks, increasing the diameter and decreasing the length, creating axial traction. Conversely, when the compressed air is released, the PAM expands and gradually returns to its original state [8]. The contraction force and displacement length of the PAM depend on the internal pressure.

Despite its many favorable properties, the nonlinear behavior and high latency of PAMs present challenges in achieving precise mathematical modeling and PAM control [9], [10]. Hysteresis is a critical nonlinear characteristic commonly encountered in mechanical actuators and control systems [11]. In control and automation engineering, hysteresis in PAMs manifests as a discrepancy between the pressure-contraction relationship during pressurization and depressurization cycles [12]. Understanding and accurately modeling

this phenomenon is crucial for developing advanced control algorithms that enhance PAM performance in robotic and biomedical applications.

Previous research efforts have focused on developing various mathematical models to characterize the hysteresis and dynamic response of PAMs. These efforts include both classical and modern approaches, such as physical-based models and data-driven techniques. However, existing models may face limitations in accuracy, computational efficiency, or adaptability to different operating conditions. Among various methods for modeling the dynamic response of PAMs reported in the literature, this study focuses on four mathematical models: nonlinear autoregressive model with exogenous inputs (NARX) [13]–[16], Box-Jenkins (BJ) model [15], second order underdamped system and one zero (P2UZ) [16], and Prandtl–Ishlinskii (PI) model [17]–[19]. These models have been widely utilized to capture the dynamics of nonlinear systems.

The NARX model is particularly effective in systems with complex, nonlinear input-output relationships, as it extends the linear ARX model by incorporating nonlinearities, allowing for the detailed representation of PAM dynamics [13]. Leveraging past input and output data to predict future outputs, it provides a powerful data-driven approach for modeling PAM behavior with intricate interactions between pressure inputs and muscle contraction. The BJ model utilizes rational polynomial functions to independently parameterize dynamics and noise, making this polynomial model highly effective for discrete-time system modeling and particularly useful to compensate for noise primarily from the measurement process rather than input disturbances [15], [20], [21].

The PI model is widely recognized for its capability in hysteresis modeling. Reasons for the wide use of the classical PI model and its variants include the simplicity and flexibility in characterizing hysteresis nonlinearities [22]–[24]. It employs play operators to simulate symmetric and asymmetric hysteresis behaviors, offering a practical solution for real-time PAM control [17]–[19]. Recent advancements in PI modeling have further enhanced its accuracy and computational efficiency [24]–[27].

The P2UZ model extends the traditional second-order underdamped system by incorporating a zero into the transfer function. This enhancement improves its accuracy in modeling the oscillatory nature of PAMs. Its robustness in handling multi-frequency systems makes it particularly suitable for applications requiring precise control and stability.

This research aims to investigate the comparative effectiveness of these models in accurately capturing PAM dynamics and to gain insights into PAM hysteresis modeling across various operating conditions. To assess their performance, root mean square error (RMSE) and model fitness metrics will be utilized. The findings of this study will contribute to the development of more reliable PAM control systems, providing guidelines for selecting an appropriate hysteresis model that will ultimately advance their applications in robotics, biomedical devices, and industrial automation.

2.   METHOD
2.1. System overview

The PAM experimental setup is depicted in Figure 1. A PAM (MAS-20-200N, FESTO) with a diameter of 20 mm and an initial length of 200 mm was used. According to FESTO specifications, this PAM can shrink up to 25% at the pressure of 6 bar. Preliminary experiments showed that its maximal shrinkage of 37 mm could be achieved with a load mass of 20 kg and an input pressure of up to 5.5 bar. The position of the PAM was measured via its displacement with a proximity sensor (KTC-100, Texas Instruments). The pressure applied to the PAM was measured with an SR13002A pressure sensor whose measurable range is up to 10 bar. The compressed air was fed through a 5/3 scale directional control valve (MPYE-5-1/8-HF-101B, FESTO). A TMS320F28379D LaunchPAD (Texas Instruments C2000 microcontroller) was used to transmit measurement and control signals to and from a laptop computer (Windows 11 Home, core i5-1155G7, 16-GB RAM) executing control and measurement algorithms in Simulink environment – MATLAB 2021a. A 20-kg load was applied to the PAM in all experiments. Figure 2 illustrates the input pressure signals and corresponding PAM responses used during the calibration and testing phases. Two types of input signals were employed. The first, shown in Figure 2(a), was a 0.1 Hz triangular waveform with progressively decreasing amplitudes after each cycle, used for model calibration. The second input, shown in Figure 2(b), retained the triangular shape but introduced greater complexity and variability to assess the model's robustness under more realistic and unpredictable conditions. The resulting PAM responses are depicted in Figures 2(c) and (d), respectively. Figure 2(c) demonstrates the PAM's response to the first signal, revealing multiple hysteresis loops caused by the gradually decreasing amplitude, which makes this input particularly useful for calibrating models under varying conditions. In contrast, Figure 2(d) shows the response to the more complex input, where identical pressure levels yielded markedly different displacements. This underscores the system's nonlinear, memory-dependent behavior and highlights the necessity of such data for evaluating the generalization capability of the developed models.

2.2. PAM modeling methods

The mathematical model of the PAM can be fundamentally expressed by (1):

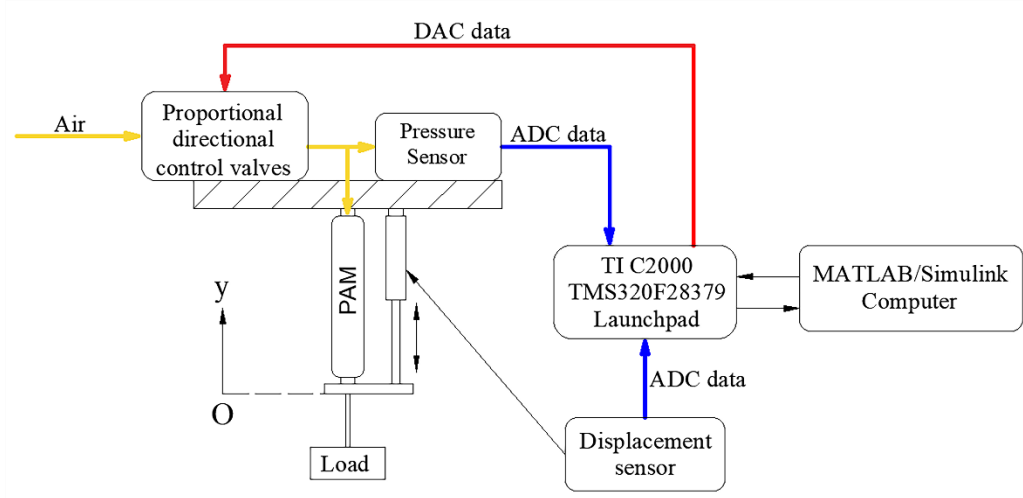$$y = f(x) = ax + b \tag{1}$$

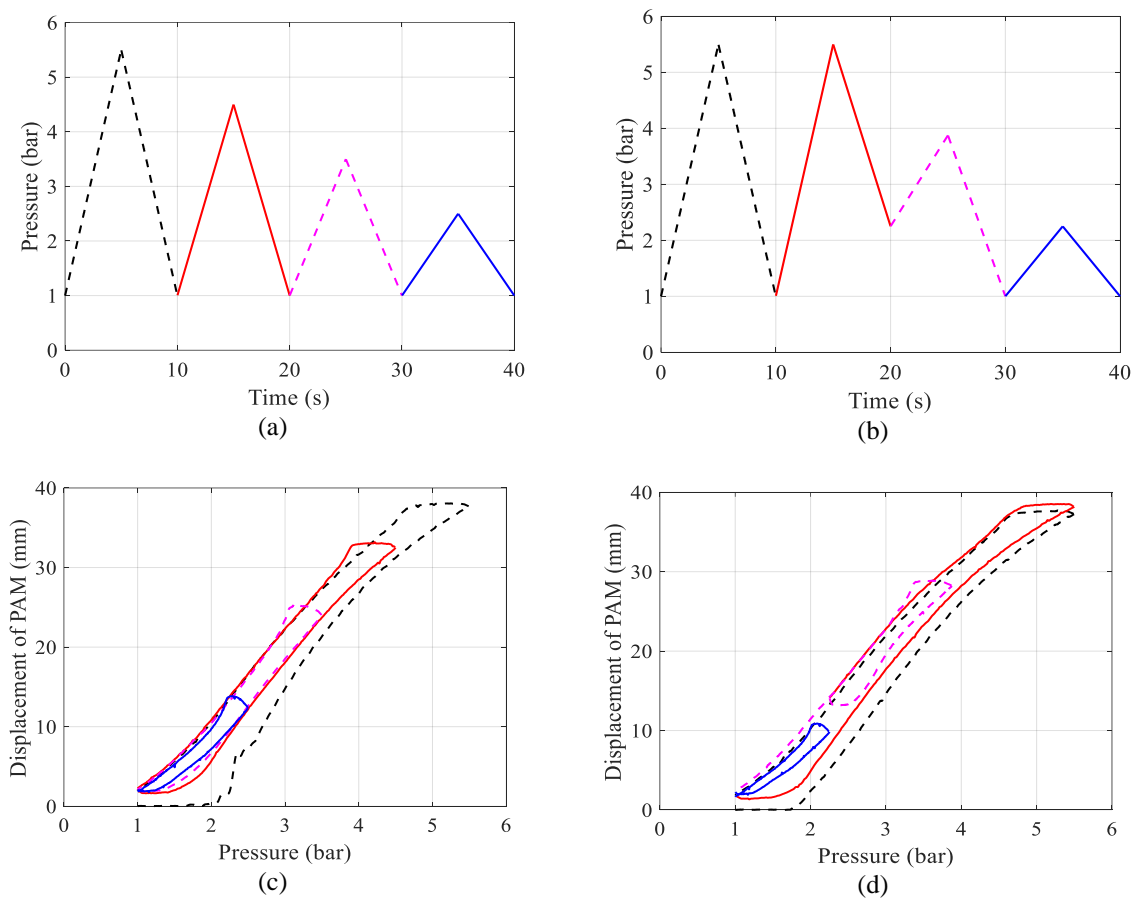Figure 1. Overview of the PAM system

Figure 2. Input signals and corresponding responses of the PAM system used for model development and testing: (a) triangular input signal with decreasing amplitude used for calibration; (b) complex input signal

with varying amplitude used for testing; (c) system response to signal (a), showing multiple hysteresis loops; and (d) system response to signal (b), highlighting nonlinear and memory-dependent behavior
where x represents the response of the investigated model among those four models under investigation in this study and b is a constant added to increase the accuracy of the model, defined as (2):

$$b = z(0) - x(0) \qquad (2)$$

where $z(0)$ and $x(0)$ denote the experimental signal and the response of the investigated model at time $t = 0$, respectively. The slope a in (1) is calculated as (3):

$$a = \frac{max\, z(0) - min\, z(0)}{max\, x(0) - min\, x(0)} \qquad (3)$$

where max(z) and min(z) represent the maximum and minimum values of the experimental signal z, respectively; max(x) and min(x) represent the maximum and minimum values of the model's response x. This adjustment aims to account for any initial discrepancies between the experimental and model-generated signals, thereby improving the accuracy and robustness of the PAM modeling. The values of parameters a and b for each mathematical model are detailed in Table 1.

These detailed methodologies provide a comprehensive overview of the various mathematical models used in this study to represent the dynamic response of PAMs. Each model offers unique advantages, contributing to a deeper understanding and more accurate prediction of PAM behavior under different experimental conditions.

Table 1. Values of parameters a and b for each mathematical model

Investigated model	a	b (mm)
P2UZ	1	10.21
Nonlinear ARX	1	2
Prandtl-Ishlinskii	1	9.03
Box-Jenkins	8.43	8.41

2.2.1. Nonlinear AutoRegressive with eXogenous input

The Nonlinear AutoRegressive with eXogenous inputs (NARX) model is a popular method for identifying and modeling nonlinear system, extending from the linear ARX model [28], with the ability to describe the nonlinear relationships between input and output variables. The NARX model is (4).

$$x(t) = f(x(t-1), x(t-2), \cdots, x(t-n), v(t-1), v(t-2), \cdots, v(t-m)) + e(t), \qquad (4)$$

where $x(t)$ and $v(t)$ are the output and input at time t, respectively; n and m denote the numbers of output and input delay, respectively; f is the NARX function; and $e(t)$ is the noise or model error. The NARX model allows the description of complex nonlinear relationships, providing high flexibility in defining nonlinear functions for effectively capturing complex dynamic PAM behaviors. System Identification Toolbox™ – MATLAB was used, in which the Adaptive Gauss-Newton method was applied for model identification.

2.2.2. Box-Jenkins Model

The BJ model is a special configuration of polynomial models that provides completely independent parameterization for dynamics and noise via rational polynomial functions. BJ models, which have always been discrete-time models, can only be estimated from data in the time domain [15]. Using a BJ model is beneficial when the noise comes primarily from the measurement process rather than from the input noise. The structure of the BJ model offers great flexibility in modeling noise due to its ability to isolate and analyze the system's dynamics independently.

The formulation of a BJ model is as (5).

$$x(t) = \sum_{nu}^{i=1} \frac{B_i(q)}{F_i(q)} v_i(t) + \frac{C(q)}{D(q)} e(t), \qquad (5)$$

where $x(t)$ and $v(t)$ are the output and input signals, $e(t)$ is the error, and B_i, C_i, F_i, and D_i are second-order polynomials, which were determined using the Box-Jenkins structure in Polynomial mode with the Adaptive Gauss-Newton method in System Identification Toolbox™ – MATLAB.

$$B(z) = 0.2377 - 0.469z^{-2}, \tag{6}$$

$$C(z) = 1 + 0.1284z^{-1} - 0.87z^{-2} \tag{7}$$

$$D(z) = 1 - 1.979z^{-1} + 0.9792z^{-2} \tag{8}$$

$$F(z) = 1 - 1.954z^{-1} + 0.9536z^{-2} \tag{9}$$

2.2.3. Second order underdamped system and one zero (P2UZ)

The standard form of the transfer function of a second-order underdamped system is (10):

$$\frac{K}{T_\omega^2 s^2 + 2\zeta T_\omega s + 1} \tag{10}$$

where $0 < \zeta < 1$ is the damping ratio. Although this underdamped system can be used to model simple oscillation, it has certain limitations when applied to more complex real-world systems with higher-order terms, resulting in low accuracy in describing the system dynamics. When the system has to receive input signals of high complexity or has a variety of frequency components, a second-order underdamped transfer function cannot provide an accurate response and adequately reflect the system behaviors [29]. To overcome these limitations, adding a zero to the model can significantly improve the accuracy and modeling capabilities of the system. For example, adding zeros enables tuning the system's frequency response and enhancing the system's response to various input signals [30]. Thus, this study modeled the PAM system using a second-order underdamped system with one zero, the transfer function of which is formulated as (11).

$$X(s) = K \frac{T_z s + 1}{(T_\omega^2 s^2 + 2\zeta T_\omega s + 1)} \tag{11}$$

The model was estimated using "Estimate Process Model" task of System Identification Toolbox™ – MATLAB (2021a version). The estimation results yielded $K = 6.7987$, $T_z = 156.3105$, $T_\omega = 5.7018$, and $\zeta = 9.1096$.

2.2.4. Prandtl-Ishlinskii model

The PI model is widely used to simulate nonlinear hysteresis, particularly for PAMs' hysteresis. As an operator-based model, it can support parallel computation, high flexibility, and facilitate integration with other dynamic factors [31]. As an operator-based model, a PI model also fits PAM hysteresis by weighting several operators called "play operators," which describe the relationship between the input pressure $v(t)$ and the output displacement $x(t)$. These operators are defined as (12) [32].

$$F_r[v, M_0](t) = max\{v(t) - r, min\{v(t) + r, F_r[v](t_{k-1})\}\} \tag{12}$$

where $v(t)$ and $F_r[v](t)$ are the input and output of the operator at time t, respectively; r is the input threshold of the play operator. The PI model uses the play operator, as defined by (12). The relationship between input pressure $v(t)$ and output displacement $x(t)$ is formulated as (13) [25].

$$x(t) = p_0 v(t) + \sum_{i=1}^{n} p_i F_r^i[v](t) \tag{13}$$

where $p_i > 0$ is the weight of the i-th play operator F_r^i with the threshold value r_i, and n is the number of play operators empirically defined from the experimental data.

The thresholds r_i are determined based on significant changes in the nonlinearity between the input and output characteristics of the PAM system observed from the experimental data. These thresholds are determined by dividing the hysteresis loop into several characteristic segments; each is considered a line segment with a slope S_i significantly different from the previous line segment. The slope S_i of each segment is computed as (14).

$$S_i = \frac{x_i - x_{i-1}}{r_i - r_{i-1}} \tag{14}$$

where x_i and x_{i-1} are the displacement values corresponding to thresholds r_i and r_{i-1} for two consecutive segments. A larger slope corresponds to a large PAM displacement due to the input pressure, indicating a stronger system response in the corresponding segment. The weight p_i can be determined from the slope as (15) [26].

$$S_i = \sum_{g=1}^{i} p_{g-1}, \quad \text{for } i = 1, \dots, n+1 \tag{15}$$

In this study, seven "play operators" were determined. The corresponding threshold and operator weight vectors are as (16) and (17).

$$r = [0 \quad 0.3392 \quad 0.6654 \quad 0.9917 \quad 1.3179 \quad 1.6442 \quad 1.9704] \tag{16}$$

$$p = [0.3067 \quad 0.1146 \quad 0.0895 \quad 0.0673 \quad 0.0673 \quad 0.0455 \quad 0.0261 \quad 0.0034] \tag{17}$$

2.3. Evaluation of the model performance

The model performance is evaluated via the RMSE and the response fitness. These two indicators are calculated based on the actual and estimated responses z and y, respectively. RMSE is a quantitative measure to evaluate the model accuracy, determined as (18):

$$RMSE = \sqrt{\sum_{j=1}^{N} \frac{(z(j) - y(j))^2}{N}} \tag{18}$$

where $z(j)$ and $y(j)$ are the actual and estimated responses z and y at sampling time j, respectively; N is the total number of observations.

The goodness of fit between the actual response and the model's estimate is calculated based on a fitness value derived from the statistical coefficient of determination as (19):

$$\text{fitness} = \left(1 - \frac{\sum_{j=1}^{N} [z(j) - y(j)]^2}{\sum_{j=1}^{N} [z(j) - \bar{z}]^2} \right) \times 100\% \tag{19}$$

where $\bar{z}$ is the average of $z(j)$.

3. RESULTS AND DISCUSSION

3.1. Experimental setup

In this study, two input pressure signals of triangular shapes with a frequency of 0.1 Hz and varying amplitudes from 5.5 bar to 1.0 bar were applied to the system. Preliminary experiments showed that a maximum displacement of 37 mm could be achieved within this input pressure range. The initial position of the PAM was approximately 0 mm with an initial pressure of 1.0 bar. A load of 20 kg was used in the experiment.

The experiment was conducted following as follows. In the model calibration phase, the input signal shown in Figure 2(a) was applied to the system. This signal had decreasing amplitudes after each cycle; therefore, different hysteresis loops were observed, as shown in Figure 2(c). These responses were used to develop more accurate NARX, BJ, P2UZ, and PI models under changing conditions. The procedures for developing NARX, BJ, P2UZ, and PI are introduced in section 2.2, with more detailed information being provided in [15], [26], [28], [30], respectively. The simulated responses of these models to this signal were plotted in Figure 3 to compare their performances in the model calibration phase.

In the testing phase, another input signal with higher complexity and variability, as shown in Figure 2(b), was applied to the system. Figure 2(d) shows that the PAM displacement differed significantly under the same pressure level. The simulated responses of the investigated models were also plotted as shown in Figure 4 to evaluate the robustness and adaptability of the developed models to more realistic, unpredictable conditions. These observations would contribute to more accurate modeling of the PAM hysteresis, supporting the design and automatic control of PAM systems.

3.2. Modeling results and performance evaluation

NARX, BJ, P2UZ, and PI were developed based on the input pressure signal 1 (Figure 2(a)) and the PAM displacement response (Figure 2(b)). The performances of these models are evaluated with the input signal 2. Figures 3 and 4 show the models' responses with respect to the actual PAM displacements – the experimental values, in both calibration and testing phases, respectively, with a performance summary tabulated in Table 2. It is apparent that all four investigated models demonstrated good performance with a fitness value of greater than 90%. Particularly, the P2UZ model demonstrated the best performance with the RMSE of about 1.8 mm and 1.91 mm in the calibration and testing phases, respectively. The fitness values of 97.15% and 97.31%, respectively, obtained in the calibration and testing phases, showed the effectiveness of the P2UZ model in PAM hysteresis modeling. The performance of the NARX model was comparable to the P2UZ model in terms of RMSE and fitness values (96.83% and 96.72% in the calibration and testing phases). It can be concluded that both P2UZ and NARX models accurately modeled the nonlinear characteristics between the input pressure and the PAM displacement due to the inherent PAM hysteresis.

Table 2. The RMSE index of the mathematical model compared to the experimental data of PAM

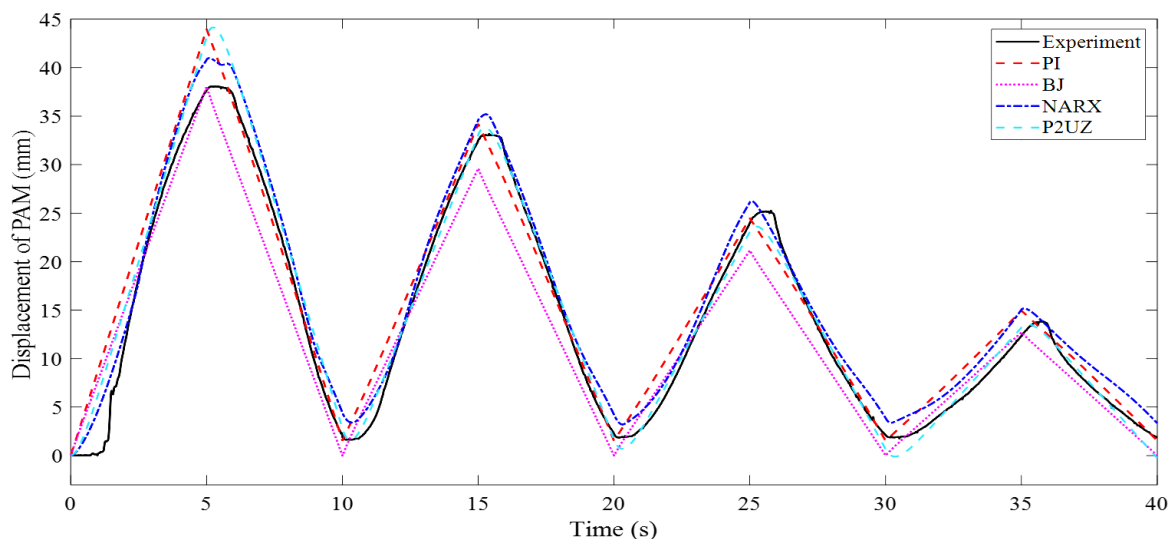| Model	Model calibration with input signal 1		Model testing with input signal 2	
	RMSE (mm)	fitness (%)	RMSE (mm)	fitness (%)
NARX	1.90	96.83	2.10	96.72
BJ	3.25	90.79	3.17	92.55
P2UZ	1.80	97.15	1.91	97.31
PI	2.60	94.08	2.48	95.44

Figure 3. Model responses and actual PAM displacement in the model calibration phase

The BJ model had the poorest performance, with the largest RMSE of about 3.25 mm and 3.17 mm in the calibration and testing phases. However, it had an acceptable fitness value of about 90.79% and 92.55% in model calibration and testing, respectively. The BJ model could not respond quickly enough in the second-half period of the reference triangular input when the amplitude is decreasing, which might lead to a larger RMSE of the BJ model compared with the other models.

The PI model showed moderate performance with calibration and testing RMSEs of 2.6 and 2.48 mm, respectively, and a considerable fitness value of 95.44% was obtained in the testing phase. Figures 3 and 4 show that the PI model stimulated good responses at the lower hysteresis loop-ends with insignificant overshoot nor undershoot. However, Figure 4 shows significant overshoots of the PI model. Because many variants of PI models have demonstrated their effectiveness in PAM hysteresis modeling [25]–[27], carefully choosing more PAM-based operators at the upper hysteresis ends can help reduce high-end-loop overshoots. The proper choice and configuration of play operators would be more complex. However, it is mathematically more difficult for the other models in this study to deal with positive and negative overshoots at the hysteresis ends.

The experimental results confirm the effectiveness of PAM modeling in achieving accurate position control under various working conditions, reinforcing its importance in this study. These findings provide valuable guidelines for selecting appropriate modeling approaches for PAMs. For applications requiring a balance between simplicity and performance, P2UZ and NARX models offer reliable options. However, when precision is paramount, a PI model or its variants should be prioritized, provided that the optimal number of play operators is determined and their configurations are properly analyzed. The study focused on a limited set of mathematical models, highlighting the need for future research to explore additional modeling approaches, including PI variants, to further enhance accuracy and applicability in real-world PAM control systems.
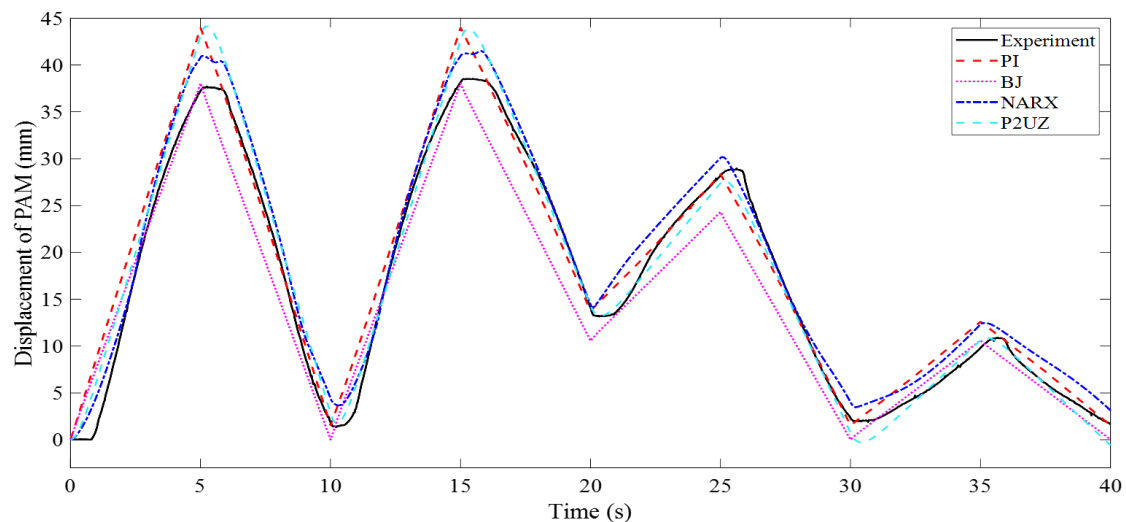

Figure 4. Model responses and actual PAM displacement in the model testing phase

4.   CONCLUSION

This study investigated four models – NARX, BJ, PI, and P2UZ – for modeling the hysteresis behavior of PAMs. The models' performance was evaluated using RMSE and fitness values, with robustness assessed across input signals of varying amplitudes. All models achieved a fitness values above 90%, indicating a general adequacy for PAM hysteresis modeling. Among them, the P2UZ model exhibited the highest accuracy (RMSE: 1.91 mm, fitness: 97.31%), followed closely by the NARX model (RMSE: 2.1 mm, fitness: 96.72%). The PI model showed moderate performance (RMSE: 2.48 mm, fitness: 95.44%), while the BJ model had the lowest accuracy (RMSE: 3.17 mm, fitness: 92.55%).

The results highlight the effectiveness of the P2UZ and NARX models as reliable, simple, and computationally efficient approaches for PAM modeling and position control. Additionally, the PI model's comparable performance achieved with a simple configuration suggests that further refinement – particularly in optimizing its play operators to mitigate overshoot at the upper hysteresis loop – could significantly enhance its accuracy. This study provides insights into selecting effective PAM modeling strategies and improving modeling accuracy for real-time control applications, including robotic actuators and prosthetic devices.

Future research should focus on optimizing the PI model for improved hysteresis compensation, potentially by dynamically adjusting its play operators in response to system behavior. Additionally, generalized PI models and the use of hysteresis inversion as a feedforward compensator could be explored to enhance closed-loop control performance. Further validation through real-time implementation in dynamic systems, such as robotic actuators and prosthetic devices, would provide valuable insights into the practical applicability and adaptability of these models.

AUTHOR CONTRIBUTIONS STATEMENT
This journal uses the Contributor Roles Taxonomy (CRediT) to recognize individual author contributions, reduce authorship disputes, and facilitate collaboration.

Name of Author	C	M	So	Va	Fo	I	R	D	O	E	Vi	Su	P	Fu
Vinh-Phuc Tran	✓	✓	✓	✓	✓	✓		✓	✓	✓	✓			
Nhut-Thanh Tran				✓	✓				✓	✓	✓			
Chi-Ngon Nguyen				✓	✓				✓	✓	✓			
Chanh-Nghiem Nguyen	✓	✓		✓	✓		✓		✓	✓	✓	✓	✓	✓

C : **C**onceptualization	I : **I**nvestigation	Vi : **Vi**sualization
M : **M**ethodology	R : **R**esources	Su : **Su**pervision
So : **So**ftware	D : **D**ata Curation	P : **P**roject administration
Va : **Va**lidation	O : Writing - **O**riginal Draft	Fu : **Fu**nding acquisition
Fo : **Fo**rmal analysis	E : Writing - Review & **E**diting	

CONFLICT OF INTEREST STATEMENT
Authors state no conflict of interest.

DATA AVAILABILITY
The data that support the findings of this study are available from the corresponding author, [Chanh-Nghiem Nguyen], upon reasonable request.

REFERENCES

[1]   S. M. Mirvakili, D. Sim, I. W. Hunter, and R. Langer, "Actuation of untethered pneumatic artificial muscles and soft robots using magnetically induced liquid-to-gas phase transitions," *Science Robotics*, vol. 5, no. 41, Apr. 2020, doi: 10.1126/SCIROBOTICS.AAZ4239.

[2]   Y. Liu, Q. Bi, X. Zang, and Y. Li, "Human-like walking of a biped robot actuated by pneumatic artificial muscles and springs," in *IEEE International Conference on Automation Science and Engineering*, Aug. 2020, vol. 2020-Augus, pp. 1395–1400, doi: 10.1109/CASE48305.2020.9216879.

[3]   W. Al-Mayahi and H. Al-Fahaam, "A review of design and modeling of pneumatic artificial muscle," *Iraqi Journal for Electrical and Electronic Engineering*, vol. 20, no. 1, pp. 122–136, Jun. 2024, doi: 10.37917/ijeee.20.1.13.

[4]   D. H. Plettenburg, "Pneumatic actuators: A comparison of energy-to-mass ratio's," in *Proceedings of the 2005 IEEE 9th International Conference on Rehabilitation Robotics*, 2005, vol. 2005, pp. 545–549, doi: 10.1109/ICORR.2005.1502022.

[5]   N. Saito, D. Furukawa, T. Satoh, and N. Saga, "Development of semi-crouching assistive device using pneumatic artificial muscle," *Journal of Robotics and Mechatronics*, vol. 32, no. 5, pp. 885–893, Oct. 2020, doi: 10.20965/jrm.2020.p0885.

[6]   T. C. Tsai and M. H. Chiang, "A lower limb rehabilitation assistance training robot system driven by an innovative pneumatic artificial muscle system," *Soft Robotics*, vol. 10, no. 1, pp. 1–16, Feb. 2023, doi: 10.1089/soro.2020.0216.

[7]   M. U. A. Khan, A. Ali, R. Muneer, and M. Faisal, "Pneumatic artificial muscle-based stroke rehabilitation device for upper and lower limbs," *Intelligent Service Robotics*, vol. 17, no. 1, pp. 33–42, Jan. 2024, doi: 10.1007/s11370-023-00509-y.

[8]   M. D. Doumit and S. Pardoel, "Dynamic contraction behaviour of pneumatic artificial muscle," *Mechanical Systems and Signal Processing*, vol. 91, pp. 93–110, Jul. 2017, doi: 10.1016/j.ymssp.2017.01.001.

[9]   V. P. Trần, H. T. T. Nguyễn, H. N. Ngô, M. K. Nguyễn, C. N. Nguyễn, and C. N. Nguyễn, "Điều khiển vị trí cơ nhân tạo khí nén sử dụng bộ điều khiển PID," *Can Tho University Journal of Science*, vol. 59, no. ETMD, pp. 45–49, May 2023, doi: 10.22144/ctu.jvn.2023.028.

[10] A. Festo, *Fluidic muscle DMSP*. 2007.

[11] J. M. Rodriguez-Fortun, J. Orus, J. Alfonso, F. Buil, and J. A. Castellanos, "Hysteresis in piezoelectric actuators: Modeling and compensation," *IFAC Proceedings Volumes (IFAC-PapersOnline)*, vol. 44, no. 1 PART 1, pp. 5237–5242, Jan. 2011, doi: 10.3182/20110828-6-IT-1002.01063.

[12] T. Vo-Minh, T. Tjahjowidodo, H. Ramon, and H. Van Brussel, "A new approach to modeling hysteresis in a pneumatic artificial muscle using the Maxwell-slip model," *IEEE/ASME Transactions on Mechatronics*, vol. 16, no. 1, pp. 177–186, Feb. 2011, doi: 10.1109/TMECH.2009.2038373.

[13] A. Kadochnikova, Y. Zhu, Z. Q. Lang, and V. Kadirkamanathan, "Integrated identification of the nonlinear autoregressive models with exogenous inputs (NARX) for engineering systems design," *IEEE Transactions on Control Systems Technology*, vol. 31, no. 1, pp. 394–401, Jan. 2023, doi: 10.1109/TCST.2022.3171130.

[14] B. Yu, D. Kim, H. Cho, and P. Mago, "A nonlinear autoregressive with exogenous inputs artificial neural network model for building thermal load prediction," *Journal of Energy Resources Technology, Transactions of the ASME*, vol. 142, no. 5, May 2020, doi: 10.1115/1.4045543.

[15] M. N. Muftah, W. L. Xuan, and A. 'Athif M. Faudzi, "ARX, ARMAX, box-jenkins, output-error, and hammerstein models for modeling intelligent pneumatic actuator (IPA) system," *Journal of Integrated and Advanced Engineering (JIAE)*, vol. 1, no. 2, pp. 81–88, Nov. 2021, doi: 10.51662/jiae.v1i2.18.

[16] D. B. Reynolds, D. W. Repperger, C. A. Phillips, and G. Bandry, "Modeling the dynamic characteristics of pneumatic muscle," *Annals of Biomedical Engineering*, vol. 31, no. 3, pp. 310–317, Mar. 2003, doi: 10.1114/1.1554921.

[17] S. L. Xie, H. T. Liu, J. P. Mei, and G. Y. Gu, "Modeling and compensation of asymmetric hysteresis for pneumatic artificial muscles with a modified generalized Prandtl–Ishlinskii model," *Mechatronics*, vol. 52, no. April 2017, pp. 49–57, Jun. 2018, doi: 10.1016/j.mechatronics.2018.04.001.

[18] X. Zang, Y. Liu, S. Heng, Z. Lin, and J. Zhao, "Position control of a single pneumatic artificial muscle with hysteresis compensation based on modified Prandtl-Ishlinskii model," *Bio-Medical Materials and Engineering*, vol. 28, no. 2, pp. 131–140, Mar. 2017, doi: 10.3233/BME-171662.

[19] S. Xie, J. Mei, H. Liu, and Y. Wang, "Hysteresis modeling and trajectory tracking control of the pneumatic muscle actuator using modified Prandtl–Ishlinskii model," *Mechanism and Machine Theory*, vol. 120, pp. 213–224, Feb. 2018, doi: 10.1016/j.mechmachtheory.2017.07.016.

[20] S. F. M. Hussein *et al.*, "Black box modelling and simulating the dynamic indoor relative humidity of a laboratory using autoregressive-moving-average (ARMA) model," *IOP Conference Series: Materials Science and Engineering*, vol. 884, no. 1, p. 012108, Jul. 2020, doi: 10.1088/1757-899X/884/1/012108.

[21] D. Piga, V. Breschi, and A. Bemporad, "Estimation of jump Box–Jenkins models," *Automatica*, vol. 120, p. 109126, Oct. 2020, doi: 10.1016/j.automatica.2020.109126.

[22] J. M. Nealis and R. C. Smith, "Model-based robust control design for magnetostrictive transducers operating in hysteretic and nonlinear regimes," *IEEE Transactions on Control Systems Technology*, vol. 15, no. 1, pp. 22–39, Jan. 2007, doi: 10.1109/TCST.2006.883235.

[23] M. Al Janaideh, S. Rakheja, and C. Y. Su, "An analytical generalized Prandtl-Ishlinskii model inversion for hysteresis compensation in micropositioning control," *IEEE/ASME Transactions on Mechatronics*, vol. 16, no. 4, pp. 734–744, Aug. 2011, doi: 10.1109/TMECH.2010.2052366.

[24] M. Al Janaideh, M. Al Saaideh, and X. Tan, "The prandtl-ishlinskii hysteresis model: fundamentals of the model and its inverse compensator [lecture notes]," *IEEE Control Systems*, vol. 43, no. 2, pp. 66–84, Apr. 2023, doi: 10.1109/MCS.2023.3234381.

[25] M. Al Saaideh and M. Al Janaideh, "On prandtl–ishlinskii hysteresis modeling of a loaded pneumatic artificial muscle," *ASME Letters in Dynamic Systems and Control*, vol. 2, no. 3, pp. 1–12, Jul. 2022, doi: 10.1115/1.4054779.

[26] Y. Zhang, H. Qi, Q. Cheng, Z. Li, and L. Hao, "Modeling and compensation of stiffness-dependent hysteresis coupling behavior for parallel pneumatic artificial muscle-driven soft manipulator," *Applied Sciences (Switzerland)*, vol. 14, no. 22, p. 10240, Nov. 2024, doi: 10.3390/app142210240.

[27] G. Ma, H. Jia, D. Xia, and L. Hao, "Hysteresis compensation and trajectory tracking control model for pneumatic artificial muscles," *Applied Sciences (Switzerland)*, vol. 14, no. 21, p. 9684, Oct. 2024, doi: 10.3390/app14219684.

[28] M. A. N. Amran, A. A. Bakar, M. H. A. Jalil, M. U. Wahyu, and A. F. H. A. Gani, "Simulation and modeling of two-level DC/DC boost converter using ARX, ARMAX, and OE model structures," *Indonesian Journal of Electrical Engineering and Computer Science*, vol. 18, no. 3, pp. 1172–1179, Jun. 2020, doi: 10.11591/ijeecs.v18.i3.pp1172-1179.

[29] A. Aleksandrov, D. Efimov, and E. Fridman, "On stability of second-order nonlinear time-delay systems without damping," in *Proceedings of the IEEE Conference on Decision and Control*, Dec. 2023, pp. 956–961, doi: 10.1109/CDC49753.2023.10383764.

[30] J. Luo, G. K. Er, and V. P. Iu, "Accurate transient response of non-smoothly nonlinear system driven by multiplicative and additive modulated stochastic excitations," *International Journal of Non-Linear Mechanics*, vol. 164, p. 104768, Sep. 2024, doi: 10.1016/j.ijnonlinmec.2024.104768.

[31] Y. Zhang, J. Gao, H. Yang, and L. Hao, "A novel hysteresis modelling method with improved generalization capability for pneumatic artificial muscles," *Smart Materials and Structures*, vol. 28, no. 10, p. 105014, Oct. 2019, doi: 10.1088/1361-665X/ab3770.

[32] A. G. Arcus and K. Lamkin-Kennard, "Modeling of a dynamic McKibben style muscle system using material properties," 2018.

BIOGRAPHIES OF AUTHORS

Vinh-Phuc Tran 🆔 📇 SC ⬡ received the degree of Engineer majoring in Mechatronics at Can Tho University in 2012. In 2018, he received a master's degree in automation and control engineering from Can Tho University. He has been a lecturer at the Faculty of Mechanical Engineering, Department of Mechatronics, Vinh Long University of Technology Education, since 2013. He is currently a Ph.D. student at Faculty of Automation Engineering, College of Engineering, Can Tho University. His research interests include mechatronics systems and automatic control. He can be contacted at email: phuctv@vlute.edu.vn.

Nhut-Thanh Tran 🆔 📇 SC ⬡ received a bachelor's degree in mechatronics from Can Tho University, Vietnam, in 2008 and an M.Eng. degree in automation from Ho Chi Minh City University of Technology, Vietnam, in 2011. He is a senior lecturer at Faculty of Automation Engineering, Can Tho University, Vietnam, since 2012. The degree of Ph.D. in engineering design was awarded by Kyoto Institute of Technology, Japan, in 2021. His research interests include automated systems, precision agriculture, spectroscopy applications, and image analysis. He can be contacted at email: nhutthanh@ctu.edu.vn.

Chi-Ngon Nguyen 🆔 📇 SC 🔾 received his bachelor's and master's degrees in electronic engineering from Can Tho University and the Vietnam National University, Ho Chi Minh City University of Technology, in 1996 and 2001, respectively. The Ph.D. degree was awarded by the University of Rostock, Germany, in 2007. Since 1996, he has worked at the Can Tho University. Currently, he is an associate professor in automation at Faculty of Automation Engineering and a Vice Chairman of the Board of Trustees of Can Tho University. He is also a nationally distinguished lecturer and a secretary of the National Council for Professorships in Electrical-Electronics and Automation. His research interests are AI applications, intelligent control, medical control, pattern recognition, classifications, computer vision, and agricultural automation. He can be contacted at email: ncngon@ctu.edu.vn.

Chanh-Nghiem Nguyen 🆔 📇 SC 🔾 received a master's degree in Mechatronics from Asian Institute of Technology, Pathumthani, Thailand, in 2007 and a Ph.D. degree from Graduate School of Engineering Science, Osaka University, Osaka, Japan, in 2012. Since 2005, he has worked at the Faculty of Automation Engineering, College of Engineering Technology, Can Tho University. He is currently an associate professor at Faculty of Automation Engineering and is in charge of Automation Laboratory. His research interests include computer vision, postharvest technologies, control systems, GNSS applications, machine learning, multispectral/hyperspectral imaging and applications. He can be contacted at email: ncnghiem@ctu.edu.vn.